



Deep mantle plumes and convective upwelling beneath the Pacific Ocean

Nicholas Schmerr^{a,b,*}, Edward Garnero^b, Allen McNamara^b

^a Department of Terrestrial Magnetism, Carnegie Institution of Washington, 5241 Broad Brand Road NW, Washington, DC 20015, USA

^b School of Earth and Space Exploration, Arizona State University, P.O. Box 874104, Tempe, AZ 85287, USA

ARTICLE INFO

Article history:

Received 3 September 2009

Received in revised form 4 March 2010

Accepted 10 March 2010

Available online 10 April 2010

Editor: Y. Ricard

Keywords:

mantle dynamics
seismic discontinuities
Pacific
SS precursors
Ontong Java Plateau
mantle plumes

ABSTRACT

Earth's mantle is thought to convect as a whole, with material flow across the upper mantle phase transitions of the mineral olivine at 410 and 660 km depth. However, the details of convection, especially mantle upwelling and plumes, are not well constrained. Here, we study seismic shear wave reflections from the underside of these temperature and composition dependent phase boundaries, which we resolve to be relatively flat beneath most of the Pacific, except under subduction regions and volcanic hotspots. The phase boundaries are closer together beneath the Hawaiian hotspot and also in a larger region of the South Pacific that is flanked by a number of volcanic hotspots. This region overlies the southern part of the large-scale low shear velocity province in the lowermost mantle. A large plume head or cluster of several plumes originating in the lowermost mantle and impinging upon the South Pacific 660 km discontinuity is consistent with observed phase boundary topography and subduction patterns. This feature may be related to large volume volcanic eruptions, such as the Cretaceous Ontong Java Plateau flood basalts, which have been proposed to originate in the South Pacific.

© 2010 Elsevier B.V. All rights reserved.

1. Introduction

Convection in Earth's interior drives tectonic forces that shape the surface of the planet. It is widely accepted that oceanic crust and lithosphere are created at mid-ocean ridges and consumed back into the planet at subduction zones, a process generally agreed to be fundamentally linked to mantle convection. Seismic tomography shows that anomalously high seismic velocities presumed to be cold subducted material (or "slabs") descend through the phase transitions of the mineral olivine near 410 and 660 km depth (van der Hilst, et al., 1997). Inversion modeling using gravity and post-glacial rebound data (Mitrova and Forte, 1997) suggests a strong viscosity increase accompanies the 660 km deep phase transition which may impede or slow the descent of some slabs (Ribe, et al., 2007). However, most slabs appear to have an ultimate fate of being subducted deep into the lower mantle, in some places to the core mantle boundary (CMB) at ~2891 km depth (Grand, et al., 1997). Upwelling mantle flow and plumes are less well understood, but should occur away from downwelling slabs. Most of Earth's hotspot volcanoes are situated above assumed return flow, giving rise to suggestions that the core–mantle boundary may be the source of mantle plumes that lead to surface hotspot volcanism (Morgan, 1971). Deciphering the dynamics and evolution of Earth's interior requires knowledge of mantle thermal structure, which can be

inferred from tomographically derived seismic wave speeds; however, this is often accomplished assuming an isochemical deep mantle, conflicting with recent work (Trampert, et al., 2004).

Earth's mantle beneath the Pacific Ocean is an ideal location to investigate mantle structure: it includes the largest single tectonic plate on Earth (the Pacific Plate) with active or recently active subduction zones defining a significant portion of the ocean's perimeter, and a number of hotspots and fast spreading mid-ocean ridges occupying its interior. Furthermore, a large number of seismic sources recorded by a growing number of increasingly available receivers surround the Pacific, enabling dense seismic wave sampling of the region. Numerous hotspots form linear chains of successively older volcanoes, thought to be the surface expression of stationary plumes of hot ascending material. For some hotspots, such as Hawaii, geochemical (Courtillot, et al., 2003; Putirka, 2005) and geophysical (Li, et al., 2000; Montelli, et al., 2006; Courtier et al., 2007b) evidence support a hot, deep mantle origin as the source of this intraplate volcanism. However, the source of magmas for many hotspots remains either uncertain or unresolved (Courtillot, et al., 2003). Whether or not plume "plumbing" is restricted to cylindrical conduits, vertical or contorted, remains in debate. Alternate possibilities for hot spot magma sources based on geochemical (Albarede and van der Hilst, 2002) or geodynamical considerations (Tackley, 2008) include isolated blobs in the lower mantle or upper mantle reservoirs (Anderson, 2006). Thus, improving our understanding of the thermal and chemical structure of the mantle beneath the Pacific will help constrain the nature of plumes within the mantle, as well as the style and mode of mantle convection within the Earth, which is necessary before the evolution of Earth's interior can be confidently deciphered.

* Corresponding author. Department of Terrestrial Magnetism, Carnegie Institution of Washington, 5241 Broad Brand Road NW, Washington, DC 20015, USA. Tel.: +1 202 478 8841; fax: +1 202 478 8821.

E-mail address: nschmerr@dtm.ciw.edu (N. Schmerr).

Lateral variations in upper mantle temperature and/or chemistry will perturb the depths of the solid-to-solid phase transitions in the dominant mantle mineral olivine. The exothermic transition of olivine (α) to wadsleyite (β) at 410 km depth (Katsura and Ito, 1989), and the endothermic dissociation of ringwoodite (γ) into Mg-perovskite (pv) and magnesiowüstite (mw) near 660 km depth (Ito and Takahashi, 1989), each produce a discontinuous increase in seismic wave velocity and density. The mantle transition zone (MTZ) is defined as the depth shell between these two major seismic discontinuities. Each discontinuity is of finite thickness that can be modified by passive upwelling flow (e.g., Solomatov and Stevenson, 1994). The Clapeyron slope (or the slope of the change in pressure associated with a change in the temperature at a phase transition boundary) of the α to β phase transition at 410 km depth is positive, and the slope of γ to pv+mw transition at 660 km depth is negative, resulting in the 410 and 660 km phase boundaries shifting in opposite directions in response to the same thermal anomaly. For example, a region of high temperature thins the MTZ. Conversely, low-temperatures will thicken the MTZ. Thus, excluding large chemical heterogeneities in the mantle, MTZ thickness variations provide an estimate of mantle temperature perturbations.

2. Seismic dataset

Here, we seismically examine the MTZ beneath the Pacific using transversely polarized shear waves that reflect from the underside of

the 410 and 660 km discontinuities, as well as the surface, midway between an earthquake and receiver. The S-wave that reflects from Earth's surface, denoted SS, arrives several hundred seconds after the discontinuity reflections (Fig. 1a). The discontinuity reflections, called SS precursors, depend on the discontinuity structure at the reflection location; perturbations in discontinuity depth incur deviations in their travel times. In contrast to other techniques for observing the discontinuities (see an extensive review by Shearer, 2000), SS waves provide a nearly complete sampling of the Earth, making them an ideal seismic probe of upper mantle discontinuities at both global and regional scales. To construct our dataset, we selected earthquakes with a moment magnitude >5.8 to ensure a high-energy SS arrival, source depths ≤ 75 km to avoid interference with near-source surface reflections (i.e., “depth phase” arrivals), and source–receiver geometries in the epicentral distance range of 80–165°. This resulted in a dataset of over 130,000 SS waveforms recorded at broadband seismic stations, that densely sample the mantle beneath the Pacific Ocean in unprecedented detail. A stringent signal-to-noise ratio criterion was employed, resulting in retention of 17,000 of the highest quality data (Fig. 1b). This regional dataset beneath the Pacific is similar in size to the entire datasets of past global studies (Flanagan and Shearer, 1998; Gu and Dziewonski, 2002) and takes advantage of EarthScope's recently deployed USArray, as well as nearly 20 years of broadband instrument seismograms available through the Incorporated Research Institutions for Seismology. The data sample a region constituting 20%

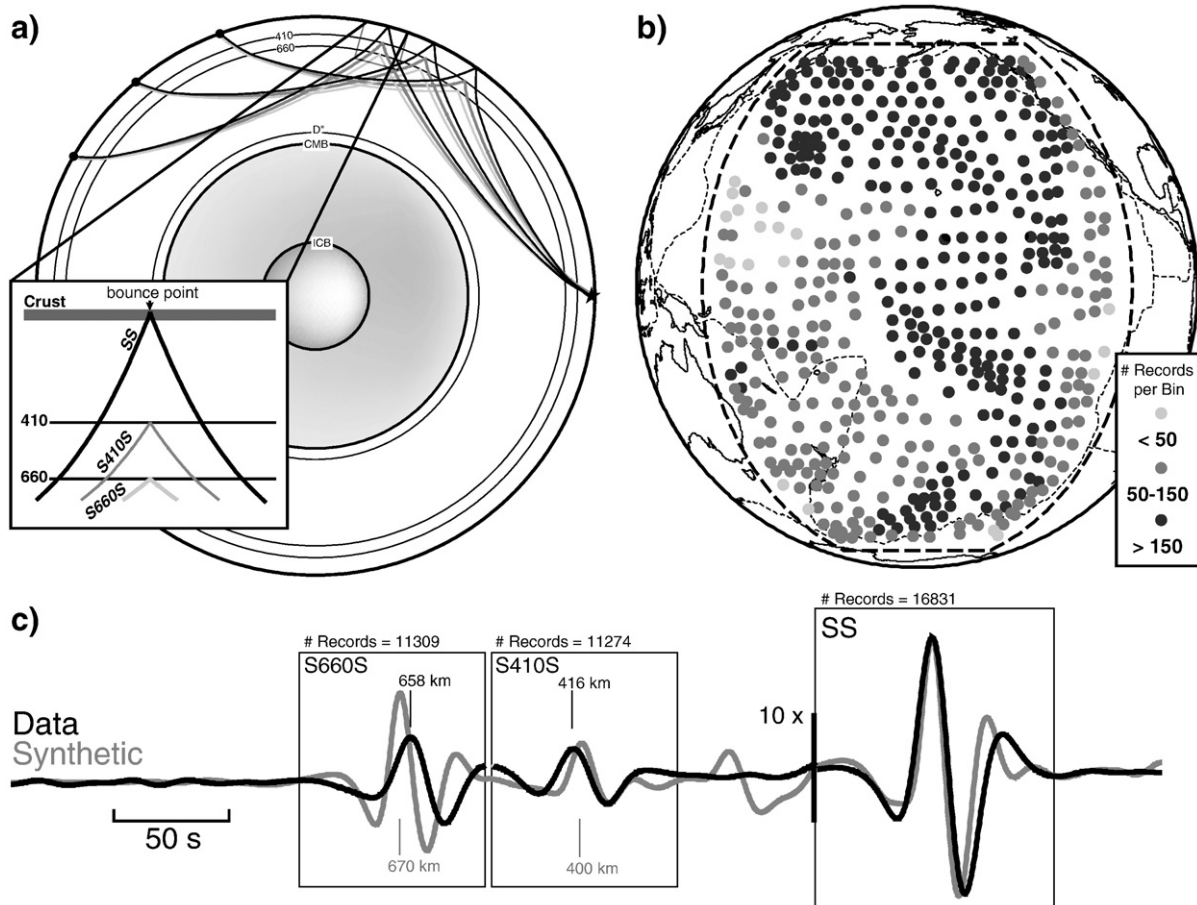


Fig. 1. Waveforms, raypaths, and sampling coverage of SS precursors beneath the Pacific Ocean. a) Seismic raypaths of SS and the precursors for epicentral distances of 110, 130, and 150°. The inset panel shows the detailed reflection point where the precursors are most sensitive to discontinuity structure (CMB = core mantle boundary; ICB = inner core/outer core boundary). b) The number of seismograms in each 1000 km radius geographic stack plotted at the average location of bounce-points falling within the bin. The extent of our study region is denoted by the thick dotted line; also shown are major plate boundaries from (Bird, 2003) (thin dotted lines). c) Summary stack of the entire Pacific dataset for both data and the corresponding PREM reflectivity synthetics. Stacks are computed for the 660 km precursor (S660S), the 410 km precursor (S410S), and SS. The number of records varies between stacks due to differing distance exclusion windows (explained in the text). Stacking the entire dataset yields average discontinuity depths for our study region of 416 km and 658 km for the 410 and 660 km discontinuities.

of Earth's surface area, and were instrumental in providing the first-ever dense sampling of the southern Pacific. Broadband data permits investigation of discontinuity topography at the shortest possible scale lengths, e.g., ≤ 1000 km lateral scales, as these instruments retain sensitivity to seismic energy at shorter wavelengths.

3. Seismic stacking method

SS precursors typically have amplitudes that are 1–10% of the SS wave, requiring the stacking of many seismograms in order to bring coherent precursory arrival energy out of the background noise (Shearer, 1990). A variety of innovative approaches for studying SS precursors exist (Deuss and Woodhouse, 2002; An, et al., 2007; Schmerr and Garnero, 2007; Houser, et al., 2008; Lawrence and Shearer, 2008). Here, we implement a stacking procedure detailed in (Schmerr and Garnero, 2006; Schmerr and Garnero, 2007), similar to the methodology of (Flanagan and Shearer, 1998), with several special considerations that allow us to assign travel time variations exclusively to the precursors, eliminating a number of effects that can contaminate or obfuscate the resulting discontinuity topography. Stacking is done with both data and reflectivity synthetic seismograms (Fuchs and Müller, 1971), where synthetics were made for each source and receiver combination to test the effects of waveform on the stacked results. Fig. 1c shows stacking results for both the Pacific dataset and corresponding PREM synthetic seismograms. To investigate regional discontinuity structure, the dataset is organized into 484 geographic bins each with a 1000 km radius. Bin locations were originally defined every 500 km on a regularly spaced grid, and are subsequently adjusted

according to the average SS bouncepoint location in each bin. The exact locations of the 484 bins used in this study are displayed in Fig. 1b and Supplemental Fig. S1. The stacks of the SS precursors off the 410 km and 660 km phase boundaries correspond to the bin location map.

We stack S410S and S660S precursors along their predicted time–distance moveouts (i.e., their “slowness”, or inverse of the seismic ray parameter) for each precursor, namely, the PREM (Dziewonski and Anderson, 1981) slownesses of S400S and S670S (Fig. 2). We use the 1-D velocity model PREM as a reference background for our study. Note that in the PREM model, the major discontinuities are at depths of 400 and 670 km (i.e., not 410 and 660 km), and hence analyses of stacks made from synthetic seismograms in this paper result in retrieving discontinuity depths at the PREM values, e.g., as in Fig. 1c. Stacking near the observed precursory slowness produces sharper, better-defined peaks for each precursor (Supplemental Fig. S2), stacking on an intermediate slowness does not significantly change the arrival times of the precursors, but slightly defocuses each precursor waveform in the stack. Thus, in this paper, we independently stack on each precursory slowness to enhance the precision of our retrieved discontinuity depths.

A primary point of concern for stacking is a variety of other seismic phases that arrive in the time window of interest and constructively or destructively interfere with the amplitudes of the SS precursors. One example includes topside reflections off the discontinuities, such as s660s_{diff} and s410s_{diff}, which directly interfere with S410S and S660S, respectively. Also, the precursors to ScSScS, i.e., ScS660ScS, cross over in time with the S410S arrival; Fig. 2c shows the time–distance behavior, i.e., the moveout, of these arrivals. We exclude particular epicentral distance and timing windows (Schmerr and Garnero, 2006) to avoid

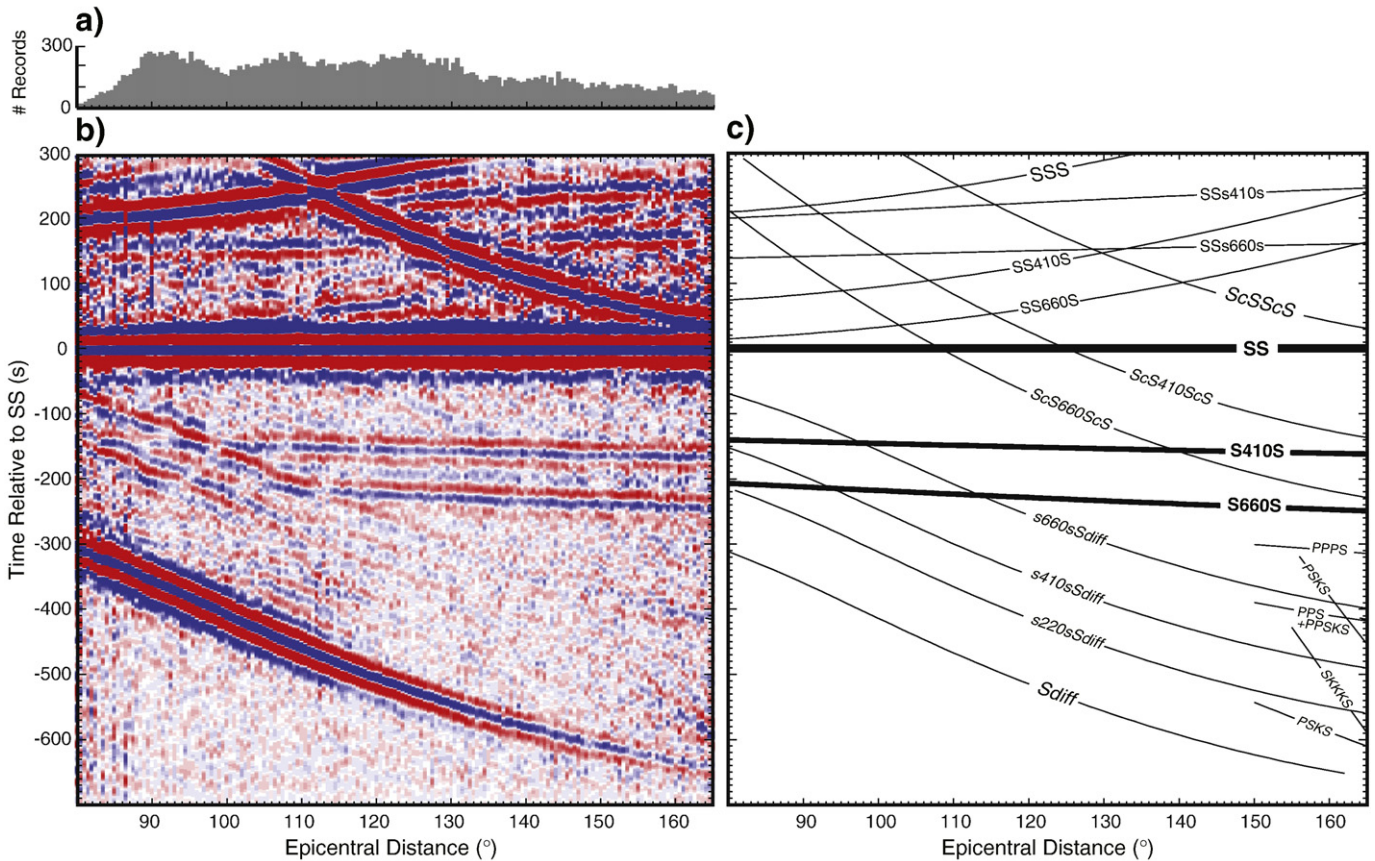


Fig. 2. The seismic wave field surrounding SS stacked in 0.5° epicentral distance bins for the Pacific dataset. a) The number of seismograms in each stack. b) Stacked seismic amplitudes where seismograms are aligned in travel time and amplitude to that of the SS arrival (shown at zero time), with the first positive swing of SS aligned on zero (positive amplitudes are blue and red amplitudes are negative). Underside reflections off the 410 and 660 km discontinuities are seen as the nearly horizontal bright arrivals between 100 and 200 s before SS. c) Predicted travel times for a variety of seismic phases near SS and the precursor wave field. Note that while this is the transverse component of motion, several vertically polarized seismic phases such as PPS and PSKS are visible.

contamination of S410S and S660S travel time perturbation estimates introduced by these additional phases (this approach is further detailed in the [Supplemental methods and Figs. S3 and S4](#)).

To further avoid contamination from non-precursory energy, we weight each seismogram in the stack based upon a signal-to-noise ratio (SNR) measurement of the SS pulse and the precursory wavefield ([Schmerr and Garnero, 2006](#)). This gives seismograms that have noise in the precursory wavefield a lower weight than those with no noise at the expected arrival time of the precursory wavefield. This is justified, as the precursors are weak arrivals compared to the SS pulse, often near the amplitude level of the noise in the seismogram. Without weighting, seismograms possessing large degrees of noise in the precursory wavefield dominate over those with very impulsive SS arrivals and relatively high SNR values. Assigning a high weight for earthquakes possessing impulsive SS signals ensures the formation of well-defined precursory arrivals from higher quality seismograms.

Our stacking approach employs a bootstrap-resampling algorithm ([Efron and Tibshirani, 1986](#)) evaluated at the 95% confidence level (2σ) that quantifies the variability (and hence reliability) of every stack and resulting discontinuity depth estimate. We apply our bootstrap histogram approach ([Schmerr and Garnero, 2007](#)) to detect multiple discontinuities and complex behavior in the stacked waveforms. In each stack, we take 300 random bootstrap resamplings of the data ([Efron and Tibshirani, 1986](#)), allowing replacement, and use the resulting set of stacked seismograms to evaluate the 2σ confidence interval for amplitudes that fall above zero at each discrete point in time. Stacked amplitudes that satisfy this requirement are termed “robust.” In general, the robustness of each stack is strongly dependent upon the number of seismograms used in each stack (see [Supplemental methods and Supplemental Fig. S5](#)). In addition to amplitude, we measure the travel time of the maximum amplitude falling within ± 15 s of the predicted precursory travel time on each of the random bootstrap resampled stacks. This allows the construction of a histogram of the travel time estimates of a given precursor (for every bin). These times are converted to depth by introducing theoretical reflectors within the PREM model above, below, and throughout the transition zone (and interpolating travel times for depths between these layers ([Schmerr and Garnero, 2006](#))), then comparing the observations to the predictions. The histogram approach allows the detection of multiple discontinuities, if present (e.g., [Deuss and Woodhouse, 2002](#)), and also provides a measure of the spread in the depth of the discontinuity and presumably the noise in the stack.

Owing to the low amplitude nature of the precursors, it is necessary to use a reference phase to align and stack the data. This reference phase is the SS arrival, as it has a raypath, slowness, and waveform that is highly similar to the S410S and S660S underside reflections that arrive several hundred seconds prior ([Fig. 1](#)). The use of a differential analysis relative to a reference phase (SS) minimizes possible travel time perturbations, such as earthquake source mislocation and/or heterogeneous structure along the raypaths, but does not necessarily account for all of the travel time differences between SS and the precursors. This complicates mapping the precursory travel times into discontinuity depths, as the SS phase accrues travel time perturbations from heterogeneity in the upper mantle and crust directly beneath the SS bouncepoint and above the S410S and S660S underside reflections. Several studies have used a joint inversion for both upper mantle structure and discontinuity depth to simultaneously account for the trade-off between these two parameters ([Gu and Dziewonski, 2002](#); [Houser, et al., 2008](#)).

Our approach to reduce these possible travel time biases and properly retrieve discontinuity depths is two-fold: (1) we first apply a timing correction for heterogeneous upper mantle structure as computed by ray-tracing through a tomographic model of upper mantle heterogeneity (e.g. S20RTS ([Ritsema, et al., 1999](#); [Ritsema, et al., 2004](#))), then (2) a correction for crustal thickness, surface topography, and bathymetry is applied (from model CRUST2.0 ([Bassin, et al., 2000](#))).

We observe only a 1–2 km difference in MTZ thicknesses corrected for different shear wave tomography models and observe a strong correlation between our computed corrections and the precursory travel times. The differential depth between the 410 km and 660 km precursory arrivals (i.e., the MTZ thickness) is largely free from the effects of mantle heterogeneity, and thus largely free of travel time effects, unless strong heterogeneity is isolated within the MTZ, and/or localized just below the 660 km discontinuity (where S660S is isolated from S410S and SS).

4. Discontinuity topography

Depth deviations of the 410 km and 660 km discontinuities and the thickness of the MTZ beneath the Pacific are shown in [Fig. 3](#) (the corresponding standard deviations are presented in [Supplemental Fig. S6](#)). To study frequency dependence of our result, we explore two different filters of the data: a bandpass from 15–50 s or “short” period in [Fig. 3a](#), and a bandpass from 25–50 s or “long” period in [Fig. 3b](#). At both frequencies, the majority of the MTZ beneath the Pacific has a thickness within ± 5 km of the global average of 242 km ([Fig. 3](#), white region), which is consistent with temperatures at or near the adiabat, and a relatively homogeneous chemical composition beneath these areas. Thus the global thickness of 242 km is an appropriate average value for the Pacific Ocean. These “global average” regions predominantly underlie the abyssal plains of the Pacific Ocean, and constitute over 75% of our study area. Only 5% of our study region has a thickened MTZ (blue) and is predominantly associated with subduction processes, similar to observations in past SS precursor studies ([Flanagan and Shearer, 1998](#); [Gu and Dziewonski, 2002](#)); the remaining 20% is thinned (warm colors), and is geographically associated with surface regions having hotspot volcanism; other SS precursor studies have also found thinned MTZ beneath hotspots ([Courtier et al., 2007b](#); [Deuss, 2007](#)).

4.1. Thickened mantle transition zone

A thickened MTZ beneath subduction having an elevated 410 km and deepened 660 km discontinuity is consistent with cold lithosphere subducting through the isochemical phase changes of olivine. The presence of chemical heterogeneity associated with subduction is not unexpected ([Schmerr and Garnero, 2007](#)), and may result in the phase boundaries deflecting differently from expectations based solely on thermal anomalies, but still result in a thickened MTZ. We therefore focus on MTZ thickness for these regions. At higher frequencies, we observe a thickened MTZ beneath the Cascadian subduction zone (15–20 km), the New Hebrides subduction zone (>20 km), the New Zealand subduction zone (5–10 km), and the Aleutian subduction zone (5–10 km), though this latter subduction zone lies at the edge of our study region. For comparison with past studies that use data recorded at long period instruments, we note the thickened MTZ beneath the New Zealand and Cascadian subduction zones vanishes in stacks of data that were low-pass filtered at 25 s period ([Fig. 3](#)). Stacks of data retaining shorter periods in the SS data thus bring smaller-scale discontinuity features into focus.

The Tonga–Kermadec subduction zone is the most anomalous – it is partially underlain by a thin MTZ ([Fig. 3](#)). However, the Tonga–Kermadec and New Hebrides subduction zones have rolled back to the east over the past 50 million years to their present location ([Schellart, et al., 2006](#)), and appear to have swept into a large province of South Pacific MTZ thinning located to the east. Several cross-sections through this region ([Fig. 4](#)) show that the 660 km phase boundary does indeed abruptly deepen at the intersection of the Tonga–Kermadec slab (profiles A–A' and C–C'), consistent with the slab being relatively cold, but interacting with a hotter region. This is further complicated by a bias in the upper mantle travel time corrections for SS from under-predicting the slab's presumed high velocity signature, which is not fully imaged by the tomography model in cross-section C–C' (in [Fig. 4](#)).

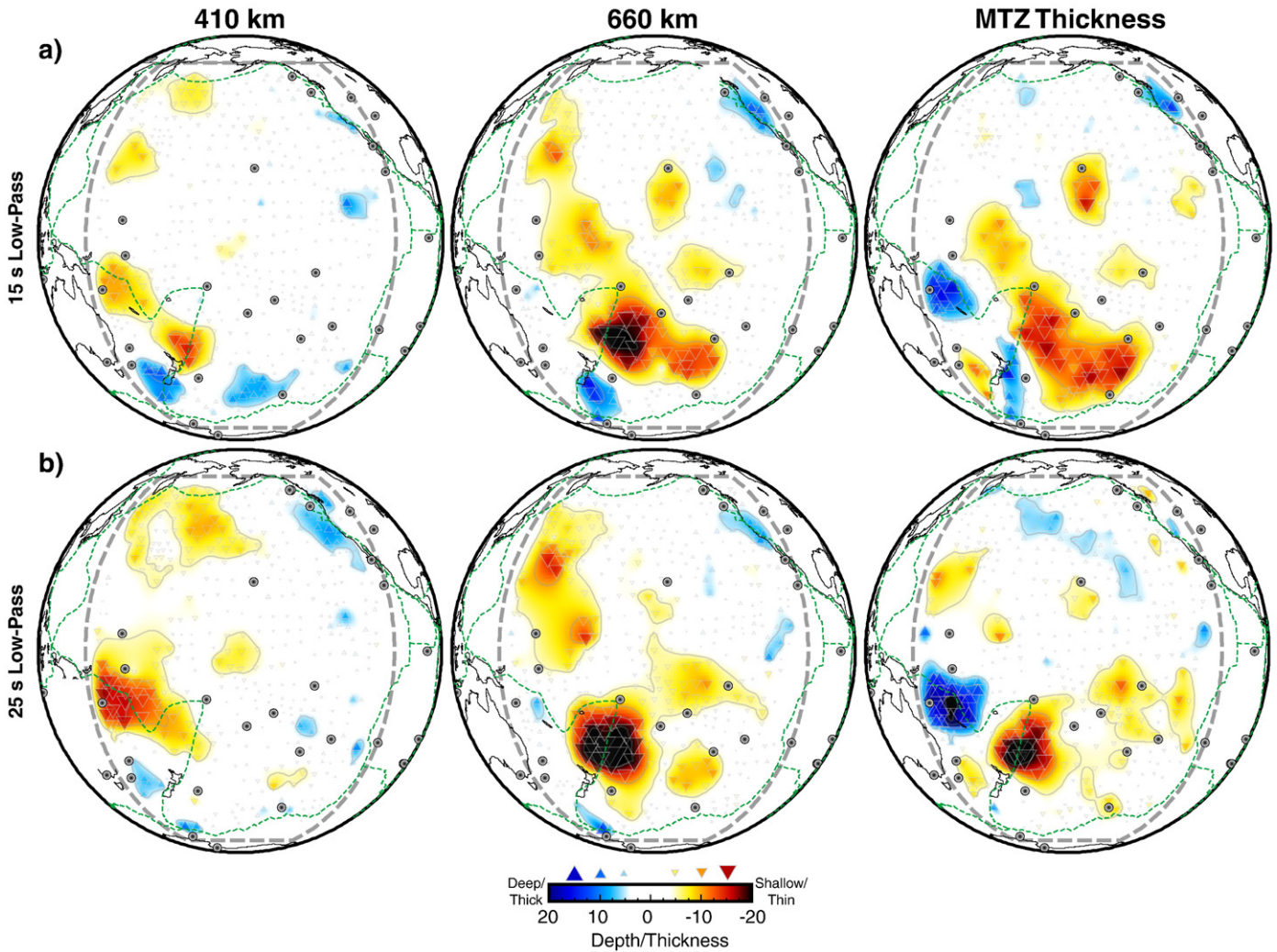


Fig. 3. Upper mantle discontinuity topography and MTZ thickness beneath the Pacific Ocean. The plate boundaries (dashed green), and geologic phenomena are shown for our study region (gray dashed outline). Hotspots (gray circles) are from (Courtillot, et al., 2003) and (Montelli, et al., 2006). Data are smoothed by a minimum-curvature gridding algorithm with a tension parameter of 0.25 (Wessel and Smith, 1998) and contoured every 5 km in depth. The triangles give the average location of bouncepoints within each stack and are scaled to the amplitude of the thickness or depth anomaly. a) Stacking results of data low-pass filtered with a corner at 15 s for the depths of 410 km and 660 km discontinuities and MTZ thickness. The scale bar indicates the amplitude of the anomalies relative to mean depths of 416 km, 658 km, and a mean thickness of 242 km. b) Stacking results of data low-pass filtered with a corner at 25 seconds for the depths of 410 km and 660 km discontinuities and MTZ thickness. Average depths and thicknesses are identical to those in panel a.

This would also result in the 660 km boundary being imaged shallower than its actual depth. High velocities associated with the slab are observed in the P-wave tomography models of this region (Li, et al., 2008). If we introduce a high velocity slab with a shear wave velocity anomaly of 3–4% into the upper mantle, we will deepen the 410 km boundary by 6–10 km, and the 660 by 12–15 km, effectively bringing the thinned region of the MTZ in line with the anomaly further east, and thickening the MTZ to the west, beneath subduction. This is demonstrated in the cross-sections A–A' and C–C' of Fig. 4 where the blue dotted line shows our computed correction for the missing slab structure when mapped onto discontinuity depth (and MTZ thickness). A similar analysis of the upper mantle corrections for regions of thinned mantle transition zone did not identify the presence of a consistent bias from under-resolved structure (see Supplemental methods).

4.2. Thinned mantle transition zone

A major feature of the MTZ beneath the Pacific is several regions of thinning (Fig. 3). To the southeast and beneath Hawaii, the 410 km discontinuity is deepened to 421 km in a localized down-warping no more than 500–1000 km wide, detectable only at dominant periods

≤ 15 s, and isolated to only bins immediately to the east (see stacks in Supplemental Fig. S2). The 660 km discontinuity is elevated to 645–650 km over a much broader region, extending 1500–2000 km to the south-southeast of Hawaii. A thinned MTZ is also detected by other SS precursor studies (Flanagan and Shearer, 1998; Gu and Dziewonski, 2002; Schmerr and Garnero, 2006), receiver function analyses (Li, et al., 2000), and ScS reverberations (Courtier et al., 2007a) that image discontinuity depths close to the Big Island of Hawaii. The observed transition zone thinning is consistent with the presence of a warm material rising from the lower mantle beneath Hawaii through the MTZ. Over the past half-decade, several tomography studies have detected a vertically continuous, reduced seismic wave speed anomaly extending from the CMB to the surface beneath the Hawaiian hotspot (Lei and Zhao, 2006; Montelli, et al., 2006). In the cross-sections A–A' and B–B' in Fig. 4, lowered shear wave velocities associated with our thinned Hawaiian anomaly are apparent, though there is considerable variation between tomography models on the exact location of the shear wave speed anomaly. However, when wave speed is averaged within a 500 km radius cylinder of material underlying the hotspot, the top and bottom of which are bounded by the 410 and 660 km discontinuities, the MTZ is found to have lowered velocities. A deep 410 km and shallow 660 km discontinuity associated with

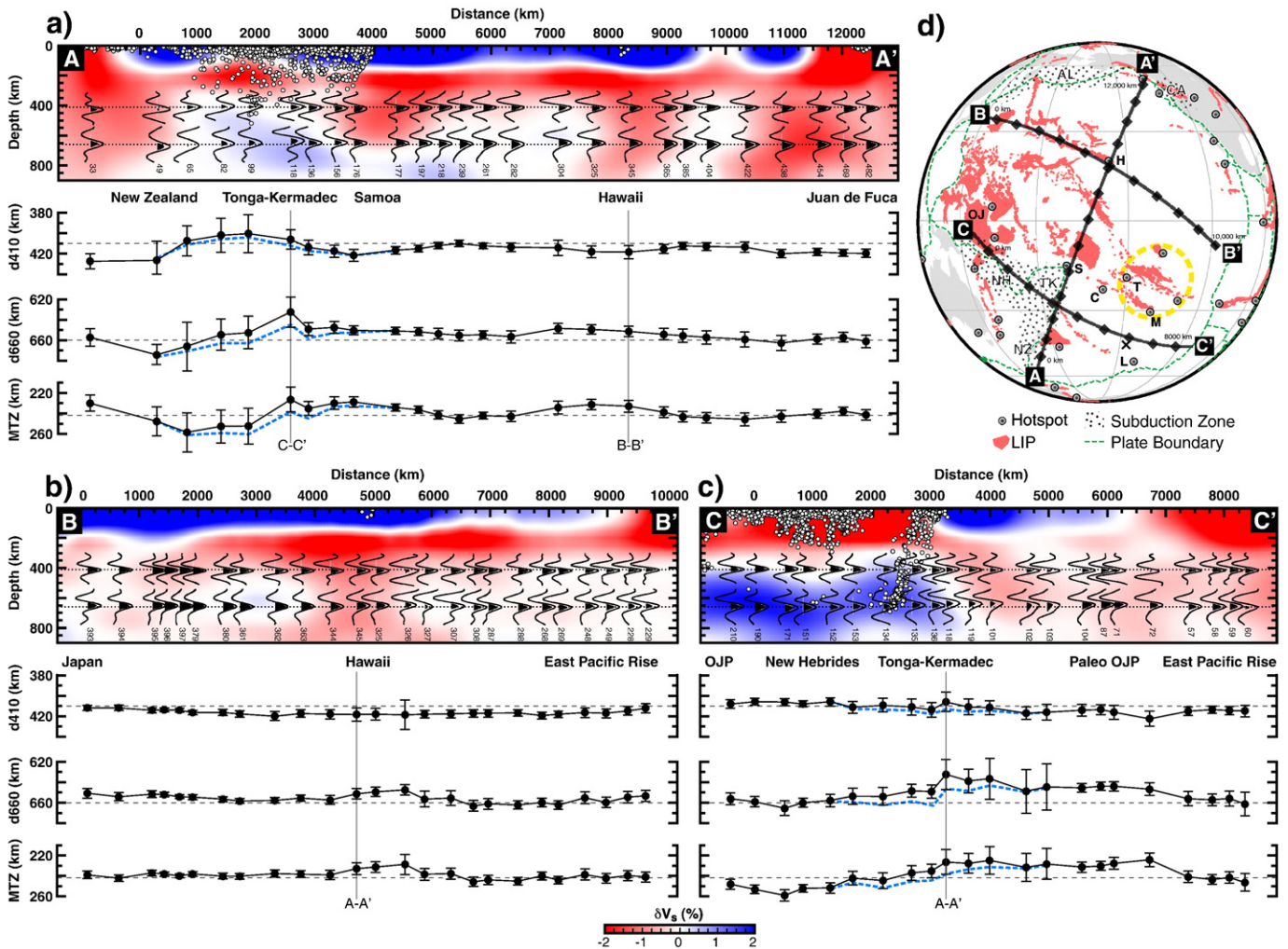


Fig. 4. Mantle cross-sections beneath several major tectonic and volcanic features in the Pacific study region. The top panel in each profile shows tomographically derived (Ritsema, et al., 2004) shear velocity perturbations (δV_s), the location of earthquakes within 500 km from the cross-section (white circles), the stacked waveforms with energy above the 95% confidence level (black shading beneath curves), and bin numbers at the bottom of each stack (corresponding to Supplemental Fig. S1). The location, waveform, and number of records in each stack are provided in Supplemental Figs. S1–S2. Beneath this panel are relative depths of each discontinuity and MTZ thickness, as well as the standard deviation of each measurement, and the intersection location of the other cross-sections. a) Cross-section A–A' extending from New Zealand to just north of the Juan de Fuca plate. b) Cross-section B–B' from the East Pacific Rise to Japan through Hawaii and parallel to the dominant motion of the Pacific plate. c) Cross-section C–C' extending from the East Pacific Rise to the Tonga–Kermadec subduction zone and Ontong Java Plateau. d) Location of the cross-sections in panels a–c, and tectonic and volcanic features within our study region: subduction regions are stippled, and named as: AL—Aleutians, CA—Cascadia, NH—New Hebrides, NZ—New Zealand, and TK—Tonga Kermadec. The yellow dashed line is the South Pacific Superswell, and hotspot labels are as follows: C—Cook, H—Hawaii, L—Louisville, M—Macdonald, S—Samoa, and T—Tahiti. “OJ” denotes the Ontong Java Plateau, a Large Igneous Province (LIP); other Pacific volcanism is red. “X” denotes the theoretical origin of the OJ (Kroenke, et al., 2004). Cross-section locations are shown with a diamond placed every 1000 km along each profile for scale.

lowered MTZ seismic velocities is well explained by a warm plume passing through the MTZ (Putirka, 2005), ultimately reaching the surface as the source for the Hawaiian hotspot. The lateral scale of this anomaly is larger than estimates based on flux considerations, e.g., 100–500 km (Sleep, 2004), which may be due to the sensitivity of SS precursors, which sample structure over a large area and hence laterally smear finer-scale features (Chaljub and Tarantola, 1997; Lawrence and Shearer, 2008). Filtering our data to 25 s dominant period, comparable to long period studies (Flanagan and Shearer, 1998), significantly reduces the amplitude of the imaged Hawaiian and the South Pacific anomalies (Fig. 3), supporting this interpretation. Not all hotspots in our study area are associated with thinned MTZ, suggesting (1) the source of volcanism is not deep-seated (Anderson, 2006), (2) the plume conduit does not pass through the MTZ directly beneath all hotspots, (3) high excess temperature plumes induce decomposition of ringwoodite into majorite (Hirose, 2002; Deuss, et al., 2006) obfuscating the presence of the plume, and/or (4) the associated plumes are too thin to detect with our method, e.g., of order 100 km across or less.

The largest anomaly of this study is the MTZ thinning by 10–25 km in the southern Pacific, in a large province roughly 4000–5000 km long and 2000–3000 km wide, beginning to the south-southwest of the Pacific Superswell and ending near the Darwin Rise (Fig. 3a). The entire province is aligned with the dominant motion of the Pacific plate. The broad scale thinning is largely due to upwarping of the 660 km discontinuity by up to 25 km, excluding the largest anomalies associated with the undercorrection for the subducting Tonga–Kermadec lithosphere. This MTZ anomaly is flanked by a number of volcanic hotspots, including Louisville, Macdonald, Tahiti, and Cook, and underlies the Samoan hotspot. While the small-scale details in tomography models differ between studies, lowered shear wave velocities are robustly found in both the deep mantle and within the MTZ for the South Pacific (Ritsema, et al., 2004), and are correlated with this region of thinned MTZ (cross-section C–C' in Fig. 4). The hotspots flanking this anomaly are characterized as having deep-rooted origins from seismic, geologic, and geochemical evidence (Courtillot, et al., 2003; Montelli, et al., 2006). This is consistent with

excess temperature responsible for the large-scale transition zone thinning we find in the South Pacific.

5. Sources of discontinuity topography

Scientists have long speculated on the relationship between hotspot volcanism and Earth’s deep mantle. Early work noted that hotspots are situated away from subduction (Morgan, 1971; Hager, et al., 1985) and over large low shear velocity provinces (LLSVPs) in the lowermost mantle beneath the Pacific and southern Africa. More recent work has identified that hotspots are far more likely to overlie the edges of the LLSVPs than the center (Thorne, et al., 2004). This result is consistent with a chemically distinct origin to LLSVPs, whereby the perimeter structure of an LLSVP can serve to guide and root mantle upwellings and plumes (Garnero and McNamara, 2008). The thermochemical LLSVPs, or “piles”, are predicted to be the hottest mantle rock on Earth, and are possibly partially molten near their margins and base (Garnero and McNamara, 2008). The observed MTZ thinning predominantly overlies the LLSVP in the Pacific (Fig. 5). The most anomalous thinning, which

occurs beneath Hawaii and the southern portion of the large South Pacific anomaly, is situated above the north and south margin, respectively, of the Pacific LLSVP. This is consistent with hot thermal upwellings and plumes guided by the edges of the chemically distinct LLSVP. Shear wave velocity reductions are more voluminous up into the lower mantle from the core–mantle boundary on the southern part of the LLSVP (Fig. 5), consistent with greater plume upwelling flux there that gives rise to the large 660 km phase boundary upwarping. Our observations connect these two features in the mantle transition zone.

The Pacific Ocean is largely surrounded by subduction, with the notable exception of the Pacific–Antarctic Ridge that defines the southern boundary of the Pacific plate. It is therefore expected that mantle plumes could more easily form within the central and southern Pacific, as predicted in geodynamical calculations that employ Earth’s subduction history as surface boundary conditions (McNamara and Zhong, 2005; Garnero and McNamara, 2008). The bottom of the transition zone marks a mantle viscosity contrast, in which the lower mantle has 1–2 orders of magnitude higher viscosity than the upper mantle (Lithgow-Bertelloni and Gurnis, 1997; Mitrova and Forte, 1997). This

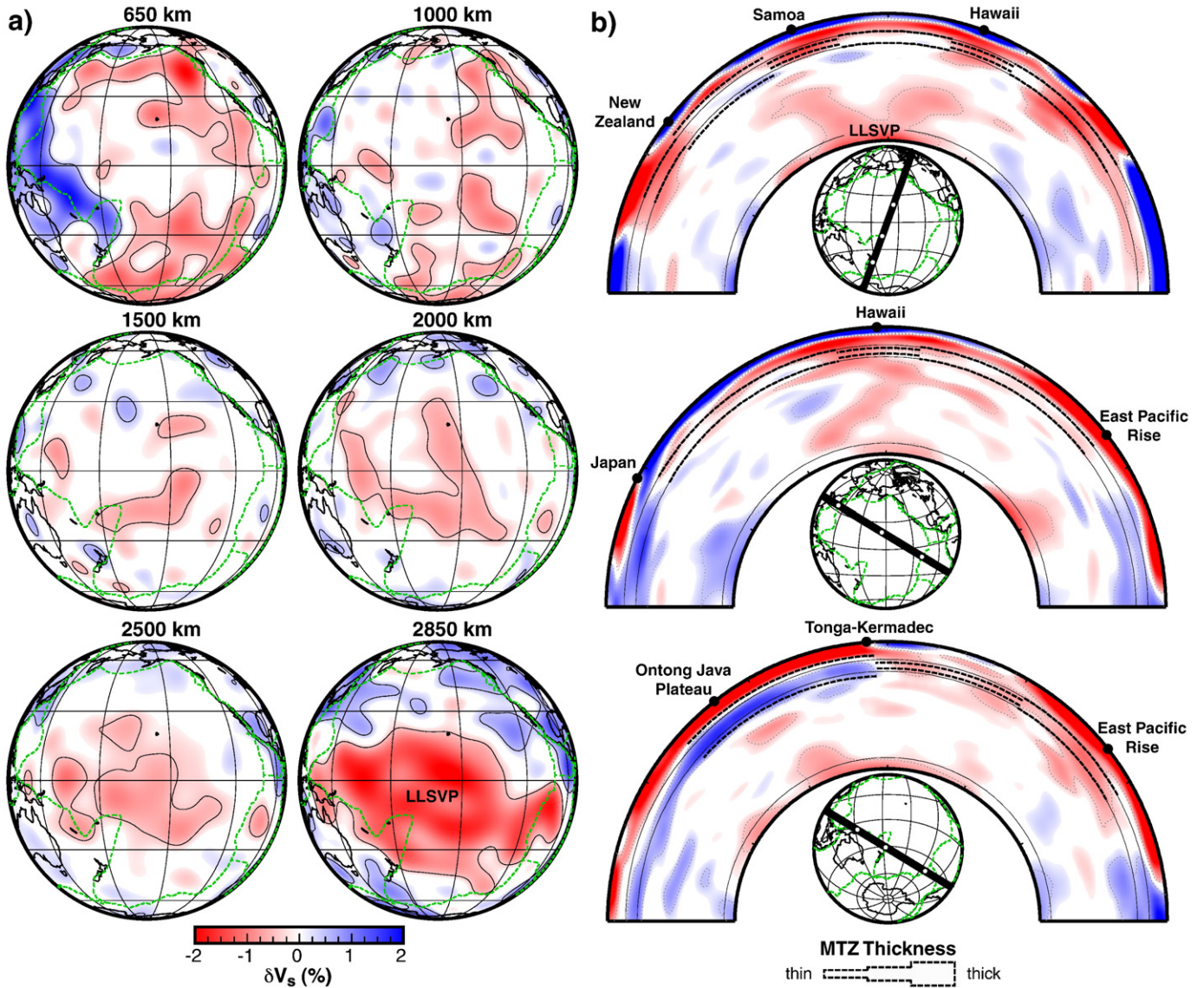


Fig. 5. The relationship of MTZ thickness to shear wave velocity heterogeneity in the mantle. a) Tomographically derived (Ritsema, et al., 2004) shear velocity perturbations at various depths within the mantle beneath our study region. The contour interval is 0.5%. b) Cross-sections through the tomographically derived shear velocities in panel a, and MTZ thickness. The locations of the cross-sections are given in the small globe underlying each panel and correspond to those presented in Fig. 4. The relative MTZ thickness beneath our study region is shown on each cross-section (dotted black lines), though the magnitude of the anomaly is greatly exaggerated to allow visualization of the thickness variations.

is expected to cause necking in mantle plumes, leading to significantly narrowed conduits in the upper mantle (van Keken and Gable, 1995). Furthermore, the endothermic phase transition associated with the 660 km may act to resist upwelling flow of hot material, perhaps leading to a small degree of bulging or ponding of plume material beneath the transition (Davies, 1995).

Plume narrowing due to the viscosity jump and possible accumulation of material due to the endothermic phase change are consistent with our results for Hawaii and the southern Pacific which display upwarping on the 660 km discontinuity on a much broader lateral scale than the depression associated with 410 km. If the large region of thinned transition zone beneath the southern Pacific is associated with plume upwelling, it is uncertain whether this is the result of a large, single plume head (Richards, et al., 1989) or a cluster of smaller plumes (Kelly and Bercovici, 1997; Schubert, et al., 2004) which could be responsible for thermally perturbing the entire region. Alternatively, these results may indicate the presence of thermochemical superplumes (Davaille, et al., 2005; Farnetani and Samuel, 2005; Samuel and Bercovici, 2006; Kumagai, et al., 2007), the tops of which may presently reside at or near the 660 km, providing the source region for smaller-scale thermal plumes that ascend through the 410 km.

To test the hypothesis of a thermal origin for our topographic variations, we correlate our MTZ thickness measurement with several tomography models. For a purely thermal origin to seismic velocity heterogeneity, low shear wave velocities correspond with higher mantle temperature and conversely high shear wave velocity with lower mantle temperature. In regions with a vertically continuous thermal anomaly across the MTZ, the thermally induced changes in seismic velocities within the MTZ should correlate with the thickness of the MTZ. Past global studies have found a weak correlation of MTZ thickness with MTZ shear velocities (Flanagan and Shearer, 1998; Deuss, 2007), though the data coverage in past studies is sparser than in our study, and the resulting resolution is longer wavelength. We also find a weak positive correlation of MTZ thickness and velocity perturbations, suggesting that beneath the Pacific, thermal variations are the primary mechanism responsible for the topographic variations seen on the MTZ discontinuities. With the exception of Tonga, subduction zones exhibit a thickened transition zone, implying colder temperatures in the MTZ. Hotspots are more complex; if we measure the average MTZ thickness within 500 km of hotspots that are classified as having geochemical and geophysical parameters consistent with an upwelling mantle plume (Courtilot, et al., 2003) and rooted in the deep mantle (>660 km depth) (Montelli, et al., 2006), we find that Hawaii, Louisville, Samoa, Marquesas and Macdonald hotspots are associated with significantly thinned MTZ. In addition, many of these hotspots lie to the edge or near our region of thin MTZ in the southern Pacific.

If the Pacific LLSVP is long-lived, then plume activity responsible for the South Pacific MTZ anomaly, whether temporally episodic or continuous, can give rise to the 660 km upwarping being similarly long-lived. The South Pacific thinned MTZ region coincides with estimates of the eruption site of the Ontong Java Plateau (OJP) in tectonic reconstructions that account for the plateau's drift over the past 120 Ma (Kroenke, et al., 2004). The OJP is the largest preserved singular magmatic event on Earth's surface, with an eruption volume on the order of $6.0 \times 10^7 \text{ km}^3$. The OJP is generally agreed to be the result of rapid decompression and large degrees melting (~30%) in the head of a newly ascended plume (Chazey and Neal, 2005), though there still remains debate over the origin of the LIP (Fitton, et al., 2004). The South Pacific MTZ anomaly is elongated in the plate motion direction, which may imply some entrainment of plume material into upper mantle flow if plate motion is coupled to flow down into the transition zone.

6. Conclusions

These observations provide geographic locations of phase boundary topography at a variety of scales. Large-scale deflections of the 660 km

discontinuity are stronger and broader than that observed for the 410 km boundary at the same locations, a result consistent with the presence of a strong viscosity change and phase transition at 660 km depth. The thinned MTZ regions appear coupled to upwelling plume processes, and are surrounded by large areas of remarkably flat phase boundaries that presently do not underlie any active tectonic processes. While these conclusions do not uniquely mandate a specific morphology of plume upwellings, they are well explained by plume structures with a geographical distribution tied to deep mantle thermochemical pile locations and a flux that is dependent on variable deep mantle pressure forces cause by the relative preponderance of subduction in the northern circum-Pacific.

Similar processes may be related to large igneous provinces in other locations. For example, the deep mantle African LLSVP is also flanked by hotspots at Earth's surface, particularly in the southern hemisphere. LIPs have been previously related to deep mantle piles (Burke, et al., 2008); high resolution MTZ imaging offers hope to assess relative plume flux differences in these regions, especially where traditional tomographic techniques do not have adequate resolution to directly image plumes. If the MTZ can be used as a witness of recent past large eruptive processes, then the opportunity exists for consideration of correlations of mass extinction events and large flood basalt eruptions (Bralower, 2008).

Acknowledgements

This study was supported by NSF grants EAR-0711401 and EAR-0453944 (N.C.S. and E.J.G) and by NSF grants EAR-0510383 and EAR-0456356 (A.K.M). All figures were plotted with the Generic Mapping Tools (Wessel and Smith, 1998). Data were obtained from the Incorporated Research Institutions for Seismology, the EarthScope USArray, and the Canadian National Seismograph Network. Data were collected using the Standing Order for Data software (Owens, et al., 2004). The TauP toolkit (Crotwell, et al., 1999) and Seismic Analysis Code were used as part of this work.

Appendix A. Supplementary data

Supplementary data associated with this article can be found in the online version at doi: [10.1016/j.epsl.2010.03.014](https://doi.org/10.1016/j.epsl.2010.03.014).

References

- Albarede, F., van der Hilst, R.D., 2002. Zoned mantle convection. *Philosophical Transactions of the Royal Society of London Series a-Math. Phys. Eng. Sci.* 360, 2569–2592.
- An, Y., Gu, Y.J., Sacchi, M.D., 2007. Imaging mantle discontinuities using least squares Radon transform. *J. Geophys. Res.-Sol. Ea.* 112.
- Anderson, D.L., 2006. Speculations on the nature and cause of mantle heterogeneity. *Tectonophysics* 416, 7–22.
- Bassin, C., Laske, G., Masters, G., 2000. The Current Limits of Resolution for Surface Wave Tomography in North America, *Eos Transactions* 81, Fall Meeting Suppl., San Francisco, CA, p. F897.
- Bird, P., 2003. An updated digital model of plate boundaries. *Geochem. Geophys. Geosyst.* 4. doi:10.1029/2001GC000252.
- Bralower, T.J., 2008. Earth science – volcanic cause of catastrophe. *Nature* 454, 285–287.
- Burke, K., Steinberger, B., Torsvik, T.H., Smethurst, M.A., 2008. Plume generation zones at the margins of large low shear velocity provinces on the core–mantle boundary. *Earth Planet. Sci. Lett.* 265, 49–60.
- Chaljub, E., Tarantola, A., 1997. Sensitivity of SS precursors to topography on the upper-mantle 660-km discontinuity. *Geophys. Res. Lett.* 24, 2613–2616.
- Chazey, W.J., Neal, C.R., 2005. Platinum-group element constraints on source composition and magma evolution of the Kerguelen Plateau using basalts from ODP Leg 183. *Geochim. Cosmochim. Acta* 69, 4685–4701.
- Courtier, A.M., Bagley, B., Revenaugh, J., 2007a. Whole mantle discontinuity structure beneath Hawaii. *Geophys. Res. Lett.* 34. doi:10.1029/2007GL031006.
- Courtier, A.M., Jackson, M.G., Lawrence, J.F., Wang, Z., Lee, C.T.A., Halama, R., Warren, J.M., Workman, R., Xu, W., Hirschmann, M.M., Larson, A.M., Hart, S.R., Lithgow-Bertelloni, C., Stixrude, L., Chen, W.P., 2007b. Correlation of seismic and petrologic thermometers suggests deep thermal anomalies beneath hotspots. *Earth Planet. Sci. Lett.* 264, 308–316.

- Courtillot, V., Davaille, A., Besse, J., Stock, J., 2003. Three distinct types of hotspots in the Earth's mantle. *Earth Planet. Sci. Lett.* 205, 295–308.
- Crotwell, H.P., Owens, T.J., Ritsema, J., 1999. The TauP toolkit: flexible seismic travel-time and ray-path utilities. *Seismol. Res. Lett.* 70, 154–160.
- Davaille, A., Stutzmann, E., Silveira, G., Besse, J., Courtillot, V., 2005. Convective patterns under the Indo-Atlantic «box». *Earth Planet. Sci. Lett.* 239, 233–252.
- Davies, G.F., 1995. Penetration of plates and plumes through the mantle transition zone. *Earth Planet. Sci. Lett.* 133, 507–516.
- Deuss, A., 2007. Seismic observations of transition-zone discontinuities beneath hotspot locations. In: Foulger, G.R., Jurdy, D.M. (Eds.), *Plates, Plumes, and Planetary Processes* 430. The Geological Society of America, Denver, pp. 121–136.
- Deuss, A., Woodhouse, J.H., 2002. A systematic search for mantle discontinuities using SS-precursors. *Geophys. Res. Lett.* 29, 1249. doi:10.1029/2002GL014768.
- Deuss, A., Redfern, S.A.T., Chambers, K., Woodhouse, J.H., 2006. The nature of the 660-kilometer discontinuity in Earth's mantle from global seismic observations of PP precursors. *Science* 311, 198–201.
- Dziewonski, A.M., Anderson, D.L., 1981. Preliminary reference earth model. *Phys. Earth Planet. In.* 25, 297–356.
- Efron, B., Tibshirani, R., 1986. Bootstrap methods for standard errors, confidence intervals, and other measures of statistical accuracy. *Stat. Sci.* 1, 54–75.
- Farnetani, C.G., Samuel, H., 2005. Beyond the thermal plume paradigm. *Geophys. Res. Lett.* 32. doi:10.1029/2005GL022360.
- Fitton, J.G., Mahoney, J.J., Wallace, P.J., Saunders, A.D., 2004. Origin and evolution of the Ontong Java Plateau: introduction. In: Fitton, J.G., Mahoney, J.J., Wallace, P.J., Saunders, A.D. (Eds.), *Origin and Evolution of the Ontong Java Plateau* 229. The Geological Society, London, pp. 1–8.
- Flanagan, M.P., Shearer, P.M., 1998. Global mapping of topography on transition zone velocity discontinuities by stacking SS precursors. *J. Geophys. Res.-Sol. Ea.* 103, 2673–2692.
- Fuchs, K., Müller, G., 1971. Computation of synthetic seismograms with the reflectivity method and comparison with observations. *Geophys. J. Roy. Astron. Soc.* 23, 417–433.
- Garnero, E.J., McNamara, A.K., 2008. Structure and dynamics of Earth's lower mantle. *Science* 320, 626–628.
- Grand, S.P., van der Hilst, R., Widiyantoro, S., 1997. Global seismic tomography: a snapshot of convection in the Earth. *GSA Today* 7, 1–7.
- Gu, Y.J., Dziewonski, A.M., 2002. Global variability of transition zone thickness. *J. Geophys. Res.-Sol. Ea.* 107, 2135. doi:10.1029/2001JB000489.
- Hager, B.H., Clayton, R.W., Richards, M.A., Comer, R.P., Dziewonski, A.M., 1985. Lower mantle heterogeneity, dynamic topography and the geoid. *Nature* 313, 541–546.
- Hirose, K., 2002. Phase transitions in pyrolytic mantle around 670 km depth: implications for upwelling of plumes from the lower mantle. *J. Geophys. Res.-Sol. Ea.* 107, 2078. doi:10.1029/2001JB000597.
- Houser, C., Masters, G., Flanagan, M.P., Shearer, P.M., 2008. Determination and analysis of long-wavelength transition zone structure using SS precursors. *Geophys. J. Int.* 174, 178–194.
- Ito, E., Takahashi, E., 1989. Postspinel transformations in the system Mg_2SiO_4 – Fe_2SiO_4 and some geophysical implications. *J. Geophys. Res.-Sol. Ea. Planet.* 94, 10637–10646.
- Katsura, T., Ito, E., 1989. The system Mg_2SiO_4 – Fe_2SiO_4 at high-pressures and temperatures – precise determination of stabilities of olivine, modified spinel, and spinel. *J. Geophys. Res.-Sol. Ea. Planet.* 94, 15663–15670.
- Kelly, A., Bercovici, D., 1997. The clustering of rising diapirs and plume heads. *Geophys. Res. Lett.* 24, 201–204.
- Kroenke, L.W., Wessel, P., Sterling, A., 2004. Motion of the Ontong Java Plateau in the hot-spot frame of reference: 122 Ma–present. In: Fitton, J.G., Mahoney, J.J., Wallace, P.J., Saunders, A.D. (Eds.), *Origin and Evolution of the Ontong Java Plateau* 229. Geological Society, London, pp. 9–20.
- Kumagai, I., Davaille, A., Kurita, K., 2007. On the fate of thermally buoyant mantle plumes at density interfaces. *Earth Planet. Sci. Lett.* 254, 180–193.
- Lawrence, J.F., Shearer, P.M., 2008. Imaging mantle transition zone thickness with SdS–SS finite-frequency sensitivity kernels. *Geophys. J. Int.* 174, 143–158.
- Lei, J.S., Zhao, D.P., 2006. A new insight into the Hawaiian plume. *Earth Planet. Sci. Lett.* 241, 438–453.
- Li, X., Kind, R., Priestley, K., Sobolev, S.V., Tilmann, F., Yuan, X., Weber, M., 2000. Mapping the Hawaiian plume conduit with converted seismic waves. *Nature* 405, 938–941.
- Li, C., van der Hilst, R.D., Engdahl, E.R., Burdick, S., 2008. A new global model for P wave speed variations in Earth's mantle. *Geochem. Geophys. Geosyst.* 9.
- Lithgow-Bertelloni, C., Gurnis, M., 1997. Cenozoic subsidence and uplift of continents from time-varying dynamic topography. *Geology* 25, 735–738.
- McNamara, A.K., Zhong, S.J., 2005. Thermochemical structures beneath Africa and the Pacific Ocean. *Nature* 437, 1136–1139.
- Mitrovica, J.X., Forte, A.M., 1997. Radial profile of mantle viscosity: results from the joint inversion of convection and postglacial rebound observables. *J. Geophys. Res.-Sol. Ea.* 102, 2751–2769.
- Montelli, R., Nolet, G., Dahlen, F.A., Masters, G., 2006. A catalogue of deep mantle plumes: new results from finite-frequency tomography. *Geochem. Geophys. Geosyst.* 7. doi:10.1029/2006GC001248.
- Morgan, W.J., 1971. Convection plumes in lower mantle. *Nature* 230, 42–43.
- Owens, T.J., Crotwell, H.P., Groves, C., Oliver-Paul, P., 2004. SOD: standing order for data. *Seismol. Res. Lett.* 75, 515–520.
- Putirka, K.D., 2005. Mantle potential temperatures at Hawaii, Iceland, and the mid-ocean ridge system, as inferred from olivine phenocrysts: evidence for thermally driven mantle plumes. *Geochem. Geophys. Geosyst.* 6. doi:10.1029/2005GC000915.
- Ribe, N.M., Stutzmann, E., Ren, Y., van der Hilst, R., 2007. Buckling instabilities of subducted lithosphere beneath the transition zone. *Earth Planet. Sci. Lett.* 254, 173–179.
- Richards, M.A., Duncan, R.A., Courtillot, V.E., 1989. Flood basalts and hot-spot tracks – plume heads and tails. *Science* 246, 103–107.
- Ritsema, J., van Heijst, H.J., Woodhouse, J.H., 1999. Complex shear wave velocity structure imaged beneath Africa and Iceland. *Science* 286, 1925–1928.
- Ritsema, J., van Heijst, H.J., Woodhouse, J.H., 2004. Global transition zone tomography. *J. Geophys. Res.-Sol. Ea.* 109. doi:10.1029/2003JB002610.
- Samuel, H., Bercovici, D., 2006. Oscillating and stagnating plumes in the Earth's lower mantle. *Earth Planet. Sci. Lett.* 248, 90–105.
- Schellart, W.P., Lister, G.S., Toy, V.G., 2006. A Late Cretaceous and Cenozoic reconstruction of the Southwest Pacific region: tectonics controlled by subduction and slab rollback processes. *Earth-Sci. Rev.* 76, 191–233.
- Schmerr, N., Garnero, E., 2006. Investigation of upper mantle discontinuity structure beneath the central Pacific using SS precursors. *J. Geophys. Res.-Sol. Ea.* 111. doi:10.1029/2005JB004197.
- Schmerr, N., Garnero, E., 2007. Upper mantle discontinuity topography from thermal and chemical heterogeneity. *Science* 318, 623–626.
- Schubert, G., Masters, G., Olson, P., Tackley, P., 2004. Superplumes or plume clusters? *Phys. Earth Planet. In.* 146, 147–162.
- Shearer, P.M., 1990. Seismic imaging of upper-mantle structure with new evidence for a 520 km discontinuity. *Nature* 344, 121–126.
- Shearer, P.M., 2000. Upper mantle discontinuities. In: Karato, S., Forte, A.M., Liebermann, R.C., Masters, G., Stixrude, L. (Eds.), *Earth's Deep Interior: Mineral Physics and Tomography from the Atomic to the Global Scale*, Geophysical Monograph 117. AGU, Washington D.C. pp. 115–131.
- Sleep, N.H., 2004. Thermal haloes around plume tails. *Geophys. J. Int.* 156, 359–362.
- Solomatov, V.S., Stevenson, D.J., 1994. Can sharp seismic discontinuities be caused by nonequilibrium phase-transformations. *Earth Planet. Sci. Lett.* 125, 267–279.
- Tackley, P.J., 2008. Geodynamics: layer cake or plum pudding? *Nat. Geosci.* 1, 157–158.
- Thorne, M.S., Garnero, E.J., Grand, S.P., 2004. Geographic correlation between hot spots and deep mantle lateral shear-wave velocity gradients. *Phys. Earth Planet. In.* 146, 47–63.
- Trampert, J., Deschamps, F., Resovsky, J., Yuen, D., 2004. Probabilistic tomography maps chemical heterogeneities throughout the lower mantle. *Science* 306, 853–856.
- van der Hilst, R.D., Widiyantoro, S., Engdahl, E.R., 1997. Evidence for deep mantle circulation from global tomography. *Nature* 386, 578–584.
- van Keken, P.E., Gable, C.W., 1995. The interaction of a plume with a rheological boundary – a comparison between 2-dimensional and 3-dimensional models. *J. Geophys. Res.-Sol. Ea.* 100, 20291–20302.
- Wessel, P., Smith, W.H.F., 1998. New, improved version of Generic Mapping Tools released. *EOS Trans. AGU.* 79, 579.